

Direct measurement of a remnant Fermi surface in SmB_6

Thomas E. Millichamp,^{1,2} David Billington,^{3,4,*} Hannah C. Roberts,¹ Jude Laverock,^{1,5}
Daniel O'Neill,⁶ Monica Ciomaga Hatnean,^{6,7,8} Geetha Balakrishnan,⁶ Jonathan
A. Duffy,⁶ Jonathan W. Taylor,⁹ Sean R. Giblin,³ and Stephen B. Dugdale^{1,†}

¹*H.H. Wills Physics Laboratory, University of Bristol,
Tyndall Avenue, Bristol, BS8 1TL, United Kingdom*

²*The Polesworth School, Dordon Road, Dordon, Tamworth, B78 1QT, United Kingdom*

³*School of Physics and Astronomy, Cardiff University,
Queen's Building, The Parade, Cardiff, CF24 3AA, United Kingdom*

⁴*Japan Synchrotron Radiation Research Institute, SPring-8, Sayo 679-5198, Japan*

⁵*School of Chemistry, University of Bristol, Cantock's Close, Bristol, BS8 1TS, United Kingdom*

⁶*Department of Physics, University of Warwick, Coventry, CV4 7AL, United Kingdom*

⁷*Materials Discovery Laboratory, Department of Materials,
Swiss Federal Institute of Technology Zurich, CH-8093 Zurich, Switzerland*

⁸*Laboratory for Multiscale materials eXperiments,
Paul Scherrer Institut, CH-5232 Villigen PSI, Switzerland*

⁹*DMSC - European Spallation Source, Universitetsparken 1, Copenhagen 2100, Denmark*

(Dated: November 16, 2021)

The quest to understand the nature of the electronic state in SmB_6 has been challenging, perplexing and surprising researchers for over half a century. In the theoretically predicted topological Kondo insulator SmB_6 [1], the nature of the bulk electronic structure is not characterised unambiguously by quantum oscillations due to contrary interpretations [2, 3]. One simple definition of an electrical insulator is a material that lacks a Fermi surface and here we report the results of our investigation into its existence in SmB_6 by Compton scattering [4]. Compton scattering measures occupied electron momentum states, is bulk sensitive due to the high energy of the incoming photons [5] and is also an ultra-fast probe of the correlated many-body electron wavefunction [6]. Remarkably, direct evidence for a three-dimensional remnant Fermi surface is observed. However, a further dichotomy is raised in that the full occupancy expected of a conventional metal is not reproduced. Our observation of a remnant Fermi surface using a momentum-resolved probe provides significant new evidence that the paradigm of a bulk insulator is not robust for SmB_6 .

The temperature dependence of the resistivity in SmB_6 led to the characterisation of the material as a hybridised f -electron Kondo insulator at low temperature. However, the recent focus on topologically nontrivial band structures has led to the claim that SmB_6 is a topological Kondo insulator [1]. As with conventional topological insulators, there should be clear evidence of surface states and, experimentally, a combination of both resistivity [7–9] and angle-resolved photoemission spectroscopy

(ARPES) [10–12] have suggested that such states are indeed present in SmB_6 . More recent measurements have further shown that the surface states are spin-polarised with the spin locked to the crystal momentum [13], as required for topologically protected states. Conversely, the exact nature of the *bulk* electronic structure is still a somewhat open question [14]. Two experiments utilising the de Haas-van Alphen (dHvA) technique have come to opposite conclusions as to the origin of the observed quantum oscillations. One reports that the angular dependence of the oscillations is evidence of 2D electron orbits associated with the surface [2], while the other finds that a 3D Fermi surface is required to explain their results [3].

Although the existence of a bulk Fermi surface may seem paradoxical for a topological Kondo insulator, there is the possibility that it could hide charge-neutral quasiparticles within the bulk [3, 15]. Investigations from a variety of techniques including muon spin relaxation (μSR) [16, 17], AC conductivity [18], neutron scattering [19, 20] and specific heat [21–23] have already found evidence for bulk in-gap excitations. These experiments do not directly probe the Fermi surface and have led to differing interpretations of the experimental data within the topological paradigm [24]. Further theoretical proposals to explain previous data include excitons [25], Majorana fermions [26] and Kondo breakdown [27], with different implications for the putative Fermi surface.

High-resolution x-ray Compton scattering probes the electron momentum density, $\rho(\mathbf{p})$, which is the probability density of electrons in momentum space (\mathbf{p} -space) [4]. The technique measures the so-called Compton profile, $J(p_z)$, which is defined as the 1D projection of $\rho(\mathbf{p})$, resolved parallel to the scattering vector, $J(p_z) = \iint \rho(\mathbf{p}) dp_x dp_y$. Compton scattering provides a unique probe of the correlated (many-body) ground-state electronic wavefunction via its underlying momentum distribution, yet is insensitive to lattice defects and atomic

* billingtond1@cardiff.ac.uk

† s.b.dugdale@bristol.ac.uk

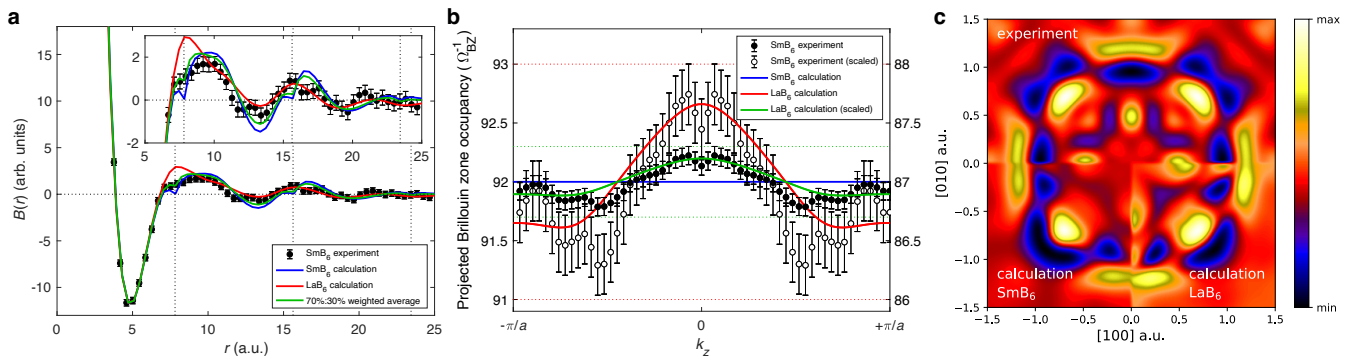


FIG. 1. **Nature of the bulk electronic state in SmB₆.** **a**, Experimental $B(r)$ for the $p_z \parallel [100]$ Compton profile of SmB₆ together with those calculated for SmB₆ (insulating), LaB₆ (metallic), and a 7 : 3 weighted average of the $B(r)$ functions for SmB₆ and LaB₆. Vertical dotted lines indicate integer multiples of the [100] lattice constant, $a = 7.815$ a.u., for which $B(r)$ must be zero for an insulator in a one-electron framework. The inset shows a magnified portion of the main panel. **b**, Experimental $\rho_{1D}(k_z)$ for the $p_z \parallel [100]$ Compton profile of SmB₆ together with those calculated for SmB₆ and LaB₆. The horizontal dotted lines are $\rho_{1D} = (N_e \pm 1)/\Omega_{BZ}$ and $\rho_{1D} = (N_e \pm 0.3)/\Omega_{BZ}$, where $N_e = 92$ and 87 for SmB₆ (left axis) and LaB₆ (right axis), respectively, and here $\Omega_{BZ} = 2\pi/a$ is the [100]-line projected 1D Brillouin zone length. Also shown are the experimental SmB₆ distribution scaled relative to N_e/Ω_{BZ} to fit the LaB₆ calculation and *vice versa*. **c**, Experimental (upper half) radial anisotropy of the (001)-plane projected $\rho_{2D}(p_x, p_y)$ of SmB₆ alongside those calculated for SmB₆ (bottom left) and LaB₆ (bottom right) to show the resemblance of the anisotropies, indicative of ellipsoidal electron Fermi surface sheets. The calculated distributions in **b** and **c** have been convoluted with 1D and 2D Gaussian functions, respectively, approximating the experimental momentum resolution. Error bars in **a** and **b** indicate statistical errors of one standard deviation, demonstrating that the observed metallic signatures are robust.

disorder. Since only occupied electronic states can contribute to $\rho(\mathbf{p})$, it also contains information about the Fermi surface in a metal. Being equally sensitive to all of the electrons means that $J(p_z)$ can be straightforwardly normalised to the number of electrons per primitive cell, $N_e \equiv \int J(p_z) dp_z \equiv \iiint \rho(\mathbf{p}) d^3\mathbf{p}$. To provide a comparison with SmB₆, we refer to isostructural LaB₆ which is a conventional, monovalent Pauli paramagnetic metal whose Fermi surface is well-known [28, 29]. Unlike SmB₆, whose anomalous properties have been associated with strong hybridisation between highly localised $4f$ states and delocalised $5d$ bands in the vicinity of the Fermi level (E_F), the $4f$ states of LaB₆ lie a few eV above E_F so are unoccupied and do not contribute to its ground state properties.

While $J(p_z)$ resides in momentum space, in real space (\mathbf{r} -space) the reciprocal form factor (which is the autocorrelation of the \mathbf{r} -space wavefunction, see Methods), $B(\mathbf{r})$, can be obtained along a particular direction through \mathbf{r} -space by taking the 1D Fourier transform of a directional Compton profile, $B(r) = \int J(p)e^{ipr} dp$. In a one-electron framework, $B(r)$ for an insulator has to be zero at non-zero integer multiples of the lattice vector, \mathbf{R} . This can be seen, for example, in the $B(r)$ functions for the weakly correlated (band) insulator, Si, and the strongly correlated (Mott) insulator, NiO (see Fig. S1 and S2, respectively, in the Supplementary information). The $B(r)$ function for the experimental $p_z \parallel [100]$ Compton profile of SmB₆ is shown in Fig. 1a together with those calculated for SmB₆ and LaB₆ which find insulating (gapped) and metallic (ungapped) ground states, re-

spectively, in agreement with similar calculations [30, 31]. In the experiment, it is evident that $B(r)$ is non-zero at integer multiples of the lattice constant, in contrast to what is predicted by the insulating SmB₆ calculation. One advantage of transforming to real space is that the impact of finite experimental momentum resolution reduces to a straightforward scaling of $B(r)$ due to the usual Fourier convolution theorem, meaning that this cannot explain their absence. The experimental $B(r)$ agrees with a metallic paradigm for SmB₆.

To further investigate the signatures of a metallic state, it is necessary to return to momentum space and back-fold (see Methods) the \mathbf{p} -space distribution, $\rho(\mathbf{p})$, into the first Brillouin zone to obtain the crystal momentum space (\mathbf{k} -space) occupation density, $\rho(\mathbf{k})$, because it is in \mathbf{k} -space that the Fermi surface exists. In 3D, the obtained $\rho(\mathbf{k})$ distribution, essentially, counts the number of electrons in occupied bands at every \mathbf{k} -point. Thus, any variation in $\rho(\mathbf{k})$ will be due the (de)population of the electron energy bands, $E_i(\mathbf{k})$, as they cross the Fermi level, E_F , at the Fermi wavevector, \mathbf{k}_F , thus revealing the presence of a Fermi surface. This back-folding procedure can be applied directly to a single directional Compton profile to obtain the 1D projected \mathbf{k} -space occupation density, $\rho_{1D}(k_z)$. Fig. 1b shows $\rho_{1D}(k_z)$ determined directly from the experimental $p_z \parallel [100]$ Compton profile of SmB₆ together with those calculated for SmB₆ (insulating) and LaB₆ (metallic). For SmB₆ the \mathbf{k} -space occupation density is flat, as expected for any insulator, because none of the bands cross E_F at any \mathbf{k} -point; any structure is a signature of partially occupied bands, *i.e.* a

metal. The experimental $\rho_{1D}(k_z)$ for SmB₆ shows clear variation with k_z and is further experimental evidence for it not being a conventional insulator. Significantly, the intensity of the experimental $\rho_{1D}(k_z)$ is suppressed to about 30% of that calculated for metallic LaB₆. We also note that the variation (near $k_z = \frac{\pi}{2a}$) is not identical to LaB₆.

Since each directional $J(p_z)$ is a 1D projection of the 3D $\rho(\mathbf{p})$, tomographic reconstruction is required to recover any integrated-over (projected) components. Here, Cormack's method, as developed by Kontrym-Sznajd [32], was used to recover one component and provide the projection of $\rho(\mathbf{p})$ onto the (001)-plane, $\rho_{2D}(p_x, p_y) = \int \rho(\mathbf{p}) dp_z$, with $p_z \parallel [001]$. The radial anisotropy (deviation from the angular average at constant momentum) of $\rho_{2D}(p_x, p_y)$, contains contributions from both the fully and any partially occupied bands. Thus, in a metal, some features will be due to the presence of the Fermi surface. The experimental radial anisotropy of $\rho_{2D}(p_x, p_y)$ for SmB₆ is shown in Fig. 1c together with those calculated for SmB₆ and LaB₆. Superficially, the majority of the features are well-matched between the experiment and both the SmB₆ and LaB₆ calculations because the dominant contributions are from similar completely filled bands. However, inspection of the experimental $\rho_{2D}(p_x, p_y)$ distribution reveals ellipsoidal features around the projected set of $\{\frac{\pi}{a}, 0\}$ -points ($\pi/a \approx 0.4$ a.u.) of the (001)-plane projected first Brillouin zone. A similar feature can be seen in LaB₆ where it has been unambiguously associated with the $\{\frac{\pi}{a}, 0, 0\}$ -centred ellipsoids of its Fermi surface [28, 29] (see Fig. S3 in the Supplementary information). In the SmB₆ experiment, there is some additional intensity in the radial anisotropy located around the projected set of $\{\frac{\pi}{a}, \frac{\pi}{a}\}$ -points which is not seen in either the insulating SmB₆ or metallic LaB₆ calculations.

On back-folding the (001)-plane projected 2D \mathbf{p} -space distribution, $\rho_{2D}(p_x, p_y)$, to \mathbf{k} -space to obtain $\rho_{2D}(k_x, k_y)$ (see Methods), the occupation density will only find an integer number electrons in occupied bands if no bands cross E_F along the projection direction. For example, the calculated Fermi surface of LaB₆ viewed down the [001] direction is shown in Fig. 2d and the corresponding (001)-plane projected $\rho_{2D}(k_x, k_y)$ is shown in Fig. 2c, with sections through $\rho_{2D}(k_x, k_y)$ along selected projected high-symmetry directions shown in Fig. 3. The (001)-plane projection of the 3D ellipsoids gives the overall structure of $\rho_{2D}(k_x, k_y)$, with the four highest intensity regions close to the projected (0,0)-point being due to the intersection of the ellipsoids, corresponding to full occupation along the projection direction at that point. Crucially, the underlying 3D Fermi surface is still visible in the 2D projection.

Fig. 2a and 3 show the experimental $\rho_{2D}(k_x, k_y)$ for SmB₆. The distribution clearly shows a remarkable departure from insulating behaviour as evidenced by the variation across the projected Brillouin zone area, as opposed to the featureless (\mathbf{k} -independent) distribution ex-

pected for an insulator. The features in $\rho_{2D}(k_x, k_y)$ are consistent with the Fermi surface proposed in the recent dHvA experiment [3], strongly resembling that of metallic LaB₆ with the signature of $\{\frac{\pi}{a}, 0, 0\}$ -centred ellipsoids [28, 29]. Additionally, occupied intensity is observed around the projected set of $\{\frac{\pi}{a}, \frac{\pi}{a}\}$ -points, suggestive of an additional Fermi surface component which has not been reported previously and which is not accessible by any simple rigid shift of the band structure relative to E_F . To extract the Fermi surface dimensions, the experimental $\rho_{2D}(k_x, k_y)$ was fitted with a 3D Fermi surface model consisting of three $\{\frac{\pi}{a}, 0, 0\}$ -centred ellipsoids and three $\{\frac{\pi}{a}, \frac{\pi}{a}, 0\}$ -centred spheres, involving just three free parameters (see Fig. S4 and S5 in the Supplementary information). Table I compares the experimental Fermi surface dimensions for SmB₆ extracted from the fit with those determined by other techniques (see Fig. S6 in the Supplementary information for a graphical comparison).

An important consideration of $\rho(\mathbf{k})$ is the *intensity* of the Fermi surface signal, which is best illustrated in Fig. 3. Intriguingly, the dynamic range of the experimental $\rho_{2D}(k_x, k_y)$ of SmB₆ is only about 91.7–92.3 Ω_{BZ}^{-1} , and integration of the dynamic range over the projected Brillouin zone area gives only 0.3 ± 0.1 electrons which, significantly, does not match the single electron contained within the half-filled Brillouin zone volume implied by the Fermi surface dimensions (see Table I). This remarkable situation does not correspond to conventional insulating or metallic behaviour. To highlight the metallic steps in the 2D projected occupancy, and how this corresponds to the 3D Fermi surface, Figs. 2b and 3 show $\rho_{2D}(k_x, k_y)$ scaled to reflect the full dynamic range of a monovalent metal (91–93 Ω_{BZ}^{-1}), similar to LaB₆ (86–88 Ω_{BZ}^{-1}), representing what we would expect to observe were it possible to realise a conventional monovalent metallic state in SmB₆ under our experimental conditions ($T = 7$ K, standard pressure and zero applied magnetic field). Similar to LaB₆, the Fermi surface of such a metal would contain exactly one conduction electron such that the Brillouin zone volume is exactly half-filled, obeying Luttinger's theorem [33]. For completeness, Fig. 3 also shows sections through the calculated flat distribution for insulating SmB₆, and the calculated $\rho_{2D}(k_x, k_y)$ for LaB₆ but with the dynamic range scaled to 86.7–87.3 Ω_{BZ}^{-1} , such that its intensity corresponds to the 0.3 electrons found in SmB₆. Thus, the *shape* of the implied 3D Fermi surface indicates that it half-fills the Brillouin zone volume and contains one electron, but the *intensity* of the observed signal indicates that it contains only 0.3 ± 0.1 electrons, in apparent violation of Luttinger's theorem.

This apparent discrepancy can perhaps be understood in terms of the mixed valence Kondo behaviour of SmB₆ at low temperature and ambient pressure. In general, Kondo insulators can be understood as half-filled (monovalent) local magnetic moment ($J \neq 0$) metals in which the conduction electrons quench the local moments by forming non-magnetic Kondo singlets ($J = 0$) below the Kondo temperature, T_K [34]. This process opens a Kondo

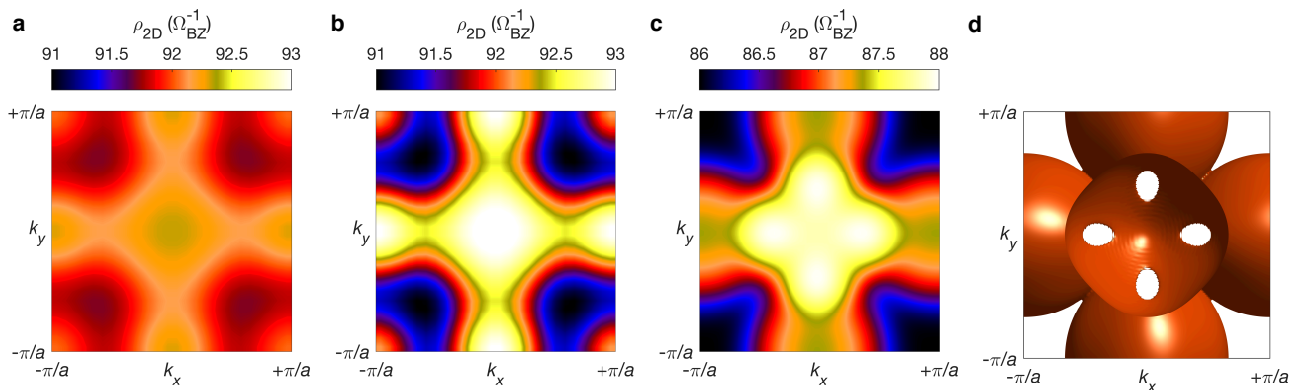


FIG. 2. **Projected occupation density of SmB₆ compared with LaB₆.** **a**, Experimental $\rho_{2D}(k_x, k_y)$ for SmB₆ showing the startling variation across the projected 2D Brillouin zone, indicating the existence of a Fermi surface. **b**, Same as **a** but with the dynamic range scaled to give what would be expected for a monovalent metal. **c**, Calculated $\rho_{2D}(k_x, k_y)$ for LaB₆ convoluted with a 2D Gaussian approximating the experimental momentum resolution. **d**, Calculated Fermi surface of LaB₆ given by the isoenergy surface $E_j(\mathbf{k}_F) = E_F$ for the single half-filled band which crosses E_F . Here, $\Omega_{BZ} = (2\pi/a)^2$ is the (001)-plane projected 2D Brillouin zone area.

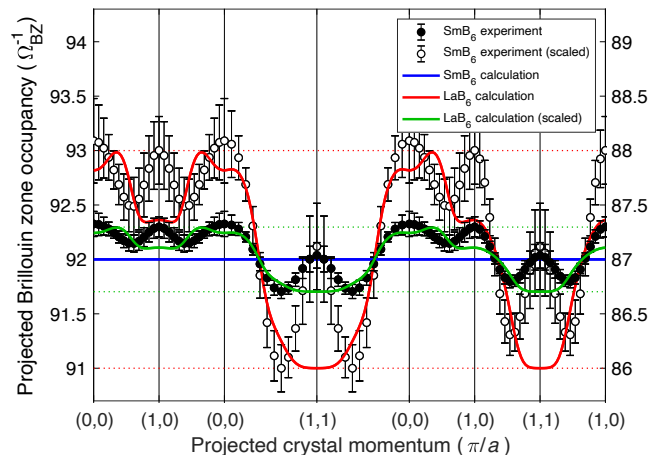


FIG. 3. **Sections through the 2D projected occupation densities.** Experimental (001)-plane projected $\rho_{2D}(k_x, k_y)$ for SmB₆ (Fig. 2a) together with those calculated for SmB₆ and LaB₆ (Fig. 2c) along selected 2D projected high-symmetry directions. The horizontal dotted lines are $(N_e \pm 1)/\Omega_{BZ}$ and $(N_e \pm 0.3)/\Omega_{BZ}$, where $N_e = 92$ and 87 electrons per primitive cell for SmB₆ (left axis) and LaB₆ (right axis), respectively, and here $\Omega_{BZ} = (2\pi/a)^2$ is the (001)-plane projected 2D Brillouin zone area. Also shown are the experimental SmB₆ distribution scaled relative to N_e/Ω_{BZ} to fit the LaB₆ calculation (Fig. 2b) and *vice versa*. The calculated distributions have been convoluted with a 2D Gaussian function approximating the experimental momentum resolution. Error bars indicate statistical errors of one standard deviation, demonstrating that the observed metallic signatures are robust.

gap at E_F with the drastic consequence of appearing as though the Fermi surface has vanished (the half-filled Brillouin zone above T_K has become completely filled below T_K). The Kondo effect can be thought of as liber-

ating a negatively charged, heavy electron which is compensated by endowing each formerly magnetic ion with an additional unit of positive charge [34], thus ensuring Luttinger's theorem [33] is not violated [35, 36].

This explanation works well in the so-called Kondo regime where the $4f$ occupation is close to integer. In SmB₆, however, inelastic neutron scattering [19], Sm L_3 -edge XAS [37] and hard x-ray $3d$ core-level photoemission spectroscopy [38] all report an average Sm valence close to +2.5 (50% Sm²⁺ and 50% Sm³⁺) at low temperatures, placing SmB₆ ($T_K \sim 100$ K [23]) firmly in the mixed valence regime. Here, the proximity of the $4f$ levels to E_F leads to dynamic charge fluctuations between non-magnetic Sm²⁺ ($4f^6$, $J_{4f} = 0$) and magnetic Sm³⁺ ($4f^5 + 5d^1$, $J_{4f} = 5/2$) states. Since the $4f^6$ spin-orbital singlet has no $4f$ moment, no Kondo effect occurs. Kondo singlet formation can only be realised for the magnetic Sm³⁺ state such that both $4f^5$ ($J_{4f} = 5/2$)

TABLE I. Comparison of 3D (bulk) and 2D (surface) experimental Fermi surface dimensions of SmB₆. The asterisk (*) indicates values determined for LaB₆.

| | $\{\frac{\pi}{a}, 0, 0\}$ ellipsoids | $\{\frac{\pi}{a}, 0, 0\}$ ellipsoids | $\{\frac{\pi}{a}, \frac{\pi}{a}, 0\}$ spheres |
|---------------------------|---|---|--|
| Technique | radius (\AA^{-1}) | radius (\AA^{-1}) | radius (\AA^{-1}) |
| Compton ^a (3D) | 0.69(8) | 0.38(12) | 0.31(15) |
| dHvA (3D) [3] | 0.69 | 0.49 | |
| dHvA (2D) [2] | | 0.30(2) | |
| ARPES (2D) [24] | 0.39(1) | 0.27(1) | |
| ARPES (2D) [12] | 0.42 | 0.29 | |
| dHvA* (3D) [29] | 0.620* | 0.489* | |

^a This work.

and $5d^1$ are present, in which case $4f^5 + 5d^1 \rightarrow [4f^5 5d^1]$ resulting in the Sm^{3+} configuration but, crucially, with $J = 0$. Indeed, Kasuya [39] argued that the mixed valence state in SmB_6 at low temperature can be viewed as a coherent fluctuation between the Sm^{2+} spin-orbital singlet and the Sm^{3+} Kondo singlet states at each Sm site, $4f^6 \equiv [4f^5 5d^1]$. Importantly, both the $4f^6$ spin-orbital singlets and the $[4f^5 5d^1]$ Kondo singlets are non-magnetic and gapped at E_F giving low temperature bulk properties that appear renormalised towards the Sm^{2+} configuration (non-magnetic, electrically insulating).

To reconcile this with our observation of a remnant Fermi surface, we argue that it must be a Kondo destroyed (magnetic) $4f^5 + 5d^1$ state with a delocalised electron that half-fills a $5d$ band which gives the remnant Fermi surface signal. More specifically, we believe this Kondo destroyed state exists as transient but spatially coherent metallic regions within the sample linked to the mixed valency of Sm in SmB_6 . The average energy lost by the photons in our Compton scattering experiment ($\Delta E \approx 35$ keV) indicates an extremely fast interaction timescale, $\tau_{\text{CS}} = h/\Delta E \sim 10^{-19}$ s, compared with other techniques such that we, essentially, measure a series of instantaneous snapshots of the fluctuating valence in which each Sm ion within the scattering volume is in the magnetic Sm^{3+} state for about 30% of the time. The 50% Sm^{2+} population is solely from the non-magnetic $4f^6$ state, while the 50% Sm^{3+} population is split between non-magnetic, Kondo insulating $[4f^5 5d^1]$ states and magnetic, metallic $4f^5 + 5d^1$ states with average populations of about 20% and 30%, respectively.

Evidence for such a state comes from a variety of techniques. Inelastic neutron scattering observes both $J_{4f} = 0 \rightarrow 1$ and $J_{4f} = 5/2 \rightarrow 7/2$ spin-flip excitations [19], with the latter excitation only attributable to the magnetic (metallic) Sm^{3+} state, and μSR measurements find magnetic fluctuations that are homogeneous, dynamic and spatially coherent up to $\xi \lesssim 100$ nm [16, 17], rather than existing as inhomogeneous spatially static regions. Remarkably, application of relatively modest hydrostatic pressure (4–10 GPa) is sufficient to completely destroy the Kondo gap in SmB_6 [40–44]. XAS has tracked the Sm^{2+} and Sm^{3+} populations as a function of pressure through the metallic transition and found that the Sm^{3+} state dominates above 10 GPa [42, 43]. Furthermore, nuclear forward scattering has measured a magnetic fraction of 30% at low temperature (3 K) and ambient pressure [40], exactly matching the metallic fraction extracted from Compton scattering, which saturates to 100% at 10 GPa [41]. In our picture of transient metallic fluctuations, we envisage that the transition under hydrostatic pressure from a mixed valence Kondo insulator to a local moment metal begins to happen when the percolation threshold is reached such that bulk electrically conducting Sm^{3+} channels start to completely extend across the macroscopic sample dimensions.

In conclusion, the variation in occupation density observed by Compton scattering matches that of in-

finately sharp steps (within the experimental momentum resolution), strongly indicative of the Fermi level lying within a band, the signature of a metallic state. The observed reduction in Fermi surface signal intensity is inconsistent with the filling of the Brillouin zone and indicates that the bulk is not completely metallic or insulating in the conventional sense. Once again, SmB_6 is seen to display an *unconventional* Fermi surface in the bulk.

Methods

Crystal growth. The SmB_6 single crystal used for this study was grown at the University of Warwick, UK, using the floating zone technique [45].

Compton scattering. In Compton scattering, monochromatic synchrotron photons are scattered incoherently from electrons in the target material. The measured distribution in energy of scattered photons is Doppler broadened as a consequence of the electron momentum component, p_z , parallel to the scattering vector. The broadened distribution is then proportional to the Compton profile, $J(p_z)$. Compton scattering was performed on beamline BL08W, SPring-8, using 115 keV monochromatic synchrotron x-rays. Measurements were performed at the base temperature of the cryostat, $T = 7$ K ($k_B T = 0.6$ meV), with standard pressure and zero applied magnetic field. Six different directions within the (001)-plane were measured, spaced equally between (and including) the [100] and [110] directions. The full-width-half-maximum momentum resolution was 0.11 a.u. at the Compton peak.

Back-folding from \mathbf{p} -space to \mathbf{k} -space. To transform the measured \mathbf{p} -space distributions to \mathbf{k} -space, the back-folding process follows the method of Lock, Crisp and West [46]. Recalling that $\mathbf{p} = \mathbf{k} + \mathbf{G}$, where \mathbf{G} is any vector of the reciprocal lattice, in 3D we can write $\rho(\mathbf{k}) = \sum_{\mathbf{G}} \rho(\mathbf{p} + \mathbf{G})$, where the (infinite) sum is over all \mathbf{G} -vectors. In a 2D projection, $\rho_{2\text{D}}(k_x, k_y) = \sum_{(G_x, G_y)} \rho_{2\text{D}}(p_x + G_x, p_y + G_y) = \int_{\Omega_{\text{BZ}}} \rho(\mathbf{k}) dk_z$, where (G_x, G_y) are the 2D projected reciprocal lattice vectors and Ω_{BZ} is the 1D projected Brillouin zone length. In a 1D projection, $\rho_{1\text{D}}(k_z) = \sum_{G_z} J(p_z + G_z) = \iint_{\Omega_{\text{BZ}}} \rho(\mathbf{k}) dk_x dk_y$, where G_z are the 1D projected reciprocal lattice vectors and Ω_{BZ} is the 2D projected Brillouin zone area. As $\rho(\mathbf{p})$ is the probability density of electrons in momentum space, once integrated over all momenta, it must equal the number of electrons per primitive cell, N_e . The same must be true even when measured in projection and subsequently back-folded into the first Brillouin zone: $N_e \equiv \iiint_{\Omega_{\text{BZ}}} \rho(\mathbf{k}) d^3\mathbf{k} \equiv \iiint \rho(\mathbf{p}) d^3\mathbf{p}$, where $\Omega_{\text{BZ}} = (2\pi/a)^3$ is the 3D Brillouin zone volume. Thus, $\rho_{2\text{D}}(k_x, k_y)$ can also be normalised such that it contains N_e electrons per primitive cell.

Counting electrons. The obtained $\rho(\mathbf{k})$ distribution can be directly related to the electron energy bands, $E_i(\mathbf{k})$, by writing $\rho(\mathbf{k}) = \sum_i n_i(\mathbf{k})$, where $n_i(\mathbf{k})$ is the occupation density of the i^{th} band at a given \mathbf{k} -point. In a one-electron framework, $n_i(\mathbf{k})$ is straightforwardly related to $E_i(\mathbf{k})$ through the

(appropriately normalised) Fermi-Dirac distribution,

$$n_i(\mathbf{k}) = \frac{2}{\Omega_{\text{BZ}}} \left[\frac{1}{\exp\left(\frac{E_i(\mathbf{k}) - E_{\text{F}}}{k_{\text{B}}T}\right) + 1} \right], \quad (1)$$

where $\Omega_{\text{BZ}} = (2\pi/a)^3$ is the 3D Brillouin zone volume, $a = 7.815$ a.u. is the cubic lattice constant, E_{F} is the Fermi level, $T = 7$ K is the temperature, k_{B} is Boltzmann's constant and the factor 2 is for spin-degeneracy. Completely filled bands, $E_i(\mathbf{k}) < E_{\text{F}}$, have $n_i(\mathbf{k}) = 2/\Omega_{\text{BZ}}$ and contain $\iiint_{\Omega_{\text{BZ}}} n_i(\mathbf{k}) d^3\mathbf{k} \equiv 2$ electrons each, contributing a flat, featureless background to $\rho(\mathbf{k})$, while completely empty bands, $E_i(\mathbf{k}) > E_{\text{F}}$, have $n_i(\mathbf{k}) = 0$ and obviously contribute nothing. It is only the partially filled bands, $E_j(\mathbf{k})$, which cross E_{F} at \mathbf{k}_{F} (defining the Fermi surface) that will abruptly change from being occupied to unoccupied, meaning that $n_j(\mathbf{k})$ will exhibit an integer step (in $2/\Omega_{\text{BZ}}$ units) at $\mathbf{k} = \mathbf{k}_{\text{F}}$, thus giving rise to any variation in $\rho(\mathbf{k})$ above the constant background. Obviously, a partially filled band contains $0 < \iiint_{\Omega_{\text{BZ}}} n_j(\mathbf{k}) d^3\mathbf{k} < 2$ electrons.

Reciprocal form factor. The reciprocal form factor, $B(\mathbf{r})$, is the autocorrelation of the \mathbf{r} -space wavefunction, $\psi(\mathbf{r})$, and is equivalently given by the 3D Fourier transform of the \mathbf{p} -space electron momentum density, $B(\mathbf{r}) \equiv \iiint \psi^*(\mathbf{r}')\psi(\mathbf{r} - \mathbf{r}') d^3\mathbf{r}' \equiv \iiint \rho(\mathbf{p})e^{i\mathbf{p}\cdot\mathbf{r}} d^3\mathbf{p}$. Importantly, $B(\mathbf{r})$ can be determined along a line in \mathbf{r} -space, say $\mathbf{r} = z$, by taking the 1D Fourier transform of the Compton profile, $B(z) = \iiint \rho(\mathbf{p})e^{ip_z z} d^3\mathbf{p} = \int J(p_z)e^{ip_z z} dp_z$. Since $\rho(\mathbf{k}) = \sum_{\mathbf{G}} \rho(\mathbf{p} + \mathbf{G})$ is constant (\mathbf{k} -independent) for an insulator in a one-electron framework, taking the Fourier transform leads directly to the result $B(\{\mathbf{R}\}) = 0$ at

non-zero integer multiples of the lattice vectors, \mathbf{R} . Thus, $B(\{\mathbf{R}\}) \neq 0$ means $\rho(\mathbf{k})$ is not \mathbf{k} -independent, indicative of metallic behaviour.

Electronic structure calculations. Density functional theory (DFT) electronic structure calculations were performed for SmB_6 and LaB_6 with the all-electron APW+I.o. code, ELK [47], using the experimental SmB_6 crystal structure [45] and a [Xe] core electron configuration for Sm and La. Convergence was realised with a $32 \times 32 \times 32$ \mathbf{k} -point grid, giving 969 distinct \mathbf{k} -points in the irreducible Brillouin zone, with an interstitial planewave cutoff determined by $R_{\text{mt}}|(\mathbf{G} + \mathbf{k})_{\text{max}}| = 8.5$, where $R_{\text{mt}} = 1.74$ a.u. is the average muffin-tin radius (the muffin-tin radii for Sm, La and B were 2.80 a.u., 2.80 a.u. and 1.56 a.u., respectively). Since Sm and La have relatively high atomic numbers, spin-orbit coupling was included in the calculations by adding a term of the form $\mathbf{S} \cdot \mathbf{L}$ (where \mathbf{S} is the spin vector and \mathbf{L} is the orbital angular momentum vector) to the second variational Hamiltonian. These calculations predict the ground state of SmB_6 to be insulating with a small indirect hybridisation gap of $\Delta \approx 3$ meV ($\Delta/k_{\text{B}} \approx 35$ K), and the ground state of LaB_6 to be metallic, and are generally in good agreement with previous calculations [30, 31]. The Fermi surface of LaB_6 was evaluated on a $64 \times 64 \times 64$ \mathbf{k} -point grid. Valence electron Compton profiles were calculated using the method of Ernstring *et al.* [48] out to $|\mathbf{p}_{\text{max}}| = 16$ a.u. for SmB_6 and $|\mathbf{p}_{\text{max}}| = 12$ a.u. for LaB_6 (see Fig. S7 in the Supplementary information for a comparison of experimental and calculated SmB_6 valence electron Compton profiles for the different crystallographic directions).

-
- [1] Dzero, M., Sun, K., Galitski, V. & Coleman, P. Topological Kondo insulators. *Phys. Rev. Lett.* **104**, 106408 (2010).
- [2] Li, G. *et al.* Two-dimensional Fermi surfaces in Kondo insulator SmB_6 . *Science* **346**, 1208–1212 (2014).
- [3] Tan, B. S. *et al.* Unconventional Fermi surface in an insulating state. *Science* **349**, 287–290 (2015).
- [4] Cooper, M. J. Compton scattering and electron momentum determination. *Reports on Progress in Physics* **48**, 415 (1985).
- [5] Dugdale, S. B. Probing the Fermi surface by positron annihilation and Compton scattering. *Low Temperature Physics* **40**, 328–338 (2014).
- [6] Cooper, M. J. Magnetic Compton scattering from HoFe_2 . *Physica B: Condensed Matter* **192**, 191 – 199 (1993).
- [7] Kim, D. J. *et al.* Surface Hall effect and nonlocal transport in SmB_6 : Evidence for surface conduction. *Scientific Reports* **3**, 3150 (2013).
- [8] Zhang, X. *et al.* Hybridization, inter-ion correlation, and surface states in the Kondo insulator SmB_6 . *Phys. Rev. X* **3**, 011011 (2013).
- [9] Kim, D. J., Xia, J. & Fisk, Z. Topological surface state in the Kondo insulator samarium hexaboride. *Nat. Mater.* **13**, 466–470 (2014).
- [10] Xu, N. *et al.* Surface and bulk electronic structure of the strongly correlated system SmB_6 and implications for a topological Kondo insulator. *Phys. Rev. B* **88**, 121102 (2013).
- [11] Neupane, M. *et al.* Surface electronic structure of the topological Kondo-insulator candidate correlated electron system SmB_6 . *Nature Communications* **4**, 2991 (2013).
- [12] Jiang, J. *et al.* Observation of possible topological in-gap surface states in the Kondo insulator SmB_6 by photoemission. *Nature Communications* **4**, 3010 (2013).
- [13] Xu, N. *et al.* Direct observation of the spin texture in SmB_6 as evidence of the topological Kondo insulator. *Nature Communications* **5**, 4566 (2014).
- [14] Zhang, R. *et al.* Understanding the quantum oscillation spectrum of heavy-fermion compound SmB_6 . *ArXiv e-prints* (2020). 2003.11052.
- [15] Chowdhury, D., Sodemann, I. & Senthil, T. Mixed-valence insulators with neutral Fermi surfaces. *Nature Communications* **9**, 1766 (2018).
- [16] Biswas, P. K. *et al.* Low-temperature magnetic fluctuations in the Kondo insulator SmB_6 . *Phys. Rev. B* **89**, 161107 (2014).
- [17] Biswas, P. K. *et al.* Suppression of magnetic excitations near the surface of the topological Kondo insulator SmB_6 . *Phys. Rev. B* **95**, 020410 (2017).
- [18] Laurita, N. J. *et al.* Anomalous three-dimensional bulk conduction within the Kondo gap of SmB_6 single crystals.

- Phys. Rev. B* **94**, 165154 (2016).
- [19] Alekseev, P. Lattice and magnetic excitations in SmB_6 . *Physica B* **186–188**, 365–371 (1993).
- [20] Fuhrman, W. T. *et al.* Interaction driven subgap spin exciton in the Kondo insulator SmB_6 . *Phys. Rev. Lett.* **114**, 036401 (2015).
- [21] Wakeham, N. *et al.* Low-temperature conducting state in two candidate topological Kondo insulators: SmB_6 and $\text{Ce}_3\text{Bi}_4\text{Pt}_3$. *Phys. Rev. B* **94**, 035127 (2016).
- [22] Hartstein, M. *et al.* Fermi surface in the absence of a Fermi liquid in the Kondo insulator SmB_6 . *Nature Physics* **14**, 166 (2017).
- [23] Phelan, W. A. *et al.* Correlation between bulk thermodynamic measurements and the low-temperature-resistance plateau in SmB_6 . *Phys. Rev. X* **4**, 031012 (2014).
- [24] Denlinger, J. D. *et al.* Consistency of photoemission and quantum oscillations for surface states of SmB_6 . *ArXiv e-prints* (2016). 1601.07408.
- [25] Knolle, J. & Cooper, N. R. Excitons in topological Kondo insulators: Theory of thermodynamic and transport anomalies in SmB_6 . *Phys. Rev. Lett.* **118**, 096604 (2017).
- [26] Baskaran, G. Majorana Fermi sea in insulating SmB_6 : A proposal and a theory of quantum oscillations in Kondo insulators. *ArXiv e-prints* (2015). 1507.03477.
- [27] Erten, O., Ghaemi, P. & Coleman, P. Kondo breakdown and quantum oscillations in SmB_6 . *Phys. Rev. Lett.* **116**, 046403 (2016).
- [28] Biasini, M. *et al.* Positron annihilation study of the electronic structure of LaB_6 and CeB_6 . *Phys. Rev. B* **56**, 10192–10199 (1997).
- [29] Harrison, N., Meeson, P., Probst, P.-A. & Springford, M. Quasiparticle and thermodynamic mass in the heavy-fermion system CeB_6 . *Journal of Physics: Condensed Matter* **5**, 7435–7450 (1993).
- [30] Antonov, V. N., Harmon, B. N. & Yaresko, A. N. Electronic structure of mixed-valence semiconductors in the LSDA+ U approximation. II. SmB_6 and YbB_{12} . *Phys. Rev. B* **66**, 165209 (2002).
- [31] Hasegawa, A. & Yanase, A. Energy bandstructure and Fermi surface of LaB_6 by a self-consistent APW method. *Journal of Physics F: Metal Physics* **7**, 1245–1260 (1977).
- [32] Kontrym-Sznajd, G. Three-dimensional image reconstruction with application in positron annihilation. *Phys. Stat. Sol. A* **117**, 227 (1990).
- [33] Luttinger, J. M. Fermi surface and some simple equilibrium properties of a system of interacting fermions. *Phys. Rev.* **119**, 1153–1163 (1960).
- [34] Coleman, P. *Heavy fermions: Electrons at the edge of magnetism, Handbook of magnetism and advanced magnetic materials*, vol. 1, 94–148 (Wiley, 2007).
- [35] Martin, R. M. Fermi-surface sum rule and its consequences for periodic Kondo and mixed-valence systems. *Phys. Rev. Lett.* **48**, 362–365 (1982).
- [36] Oshikawa, M. Topological approach to Luttinger’s theorem and the Fermi surface of a Kondo lattice. *Phys. Rev. Lett.* **84**, 3370–3373 (2000).
- [37] Mizumaki, M., Tsutsui, S. & Iga, F. Temperature dependence of Sm valence in SmB_6 studied by x-ray absorption spectroscopy. *Journal of Physics: Conference Series* **176**, 012034 (2009).
- [38] Utsumi, Y. *et al.* Bulk and surface electronic properties of SmB_6 : A hard x-ray photoelectron spectroscopy study. *Phys. Rev. B* **96**, 155130 (2017).
- [39] Kasuya, T. Mixed-valence state in SmB_6 . *Europhysics Letters* **26**, 283 (1994).
- [40] Barla, A. *et al.* High-pressure ground state of SmB_6 : Electronic conduction and long range magnetic order. *Phys. Rev. Lett.* **94**, 166401 (2005).
- [41] Derr, J. *et al.* From unconventional insulating behavior towards conventional magnetism in the intermediate-valence compound SmB_6 . *Phys. Rev. B* **77**, 193107 (2008).
- [42] Butch, N. P. *et al.* Pressure-resistant intermediate valence in the Kondo insulator SmB_6 . *Phys. Rev. Lett.* **116**, 156401 (2016).
- [43] Zhou, Y. *et al.* Quantum phase transition and destruction of Kondo effect in pressurized SmB_6 . *Science Bulletin* **62**, 1439–1444 (2017).
- [44] Chen, K. *et al.* Surface- and pressure-induced bulk Kondo breakdown in SmB_6 . *Phys. Rev. B* **97**, 235153 (2018).
- [45] Hatnean, M. C., Lees, M. R., Paul, D. M. & Balakrishnan, G. Large, high quality single-crystals of the new topological Kondo insulator, SmB_6 . *Scientific Reports* **3**, 3071 (2013).
- [46] Lock, D. G., Crisp, V. H. C. & West, R. N. Positron annihilation and Fermi surface studies: A new approach. *Journal of Physics F: Metal Physics* **3**, 561 (1973).
- [47] Sharma, S., Dewhurst, K. & Ambrosch-Draxl, C. The ELK FP-LAPW code (2004). <http://elk.sourceforge.net>.
- [48] Ernsting, D. *et al.* Calculating electron momentum densities and Compton profiles using the linear tetrahedron method. *Journal of Physics: Condensed Matter* **26**, 495501 (2014).

Acknowledgements

The Compton scattering experiments were performed with the approval of the Japan Synchrotron Radiation Research Institute (JASRI), SPring-8, proposal numbers 2016A1640 and 2019A1460. We thank Y. Sakurai (SPring-8) for sharing the Si experimental Compton scattering data. This work is supported by UK EPSRC, grant numbers EP/L015544/1 and EP/S016465/1. The crystal growth at the University of Warwick is supported by UK EPSRC, grant numbers EP/M028771/1 and EP/T005963/1.

Author contributions

T.E.M., S.R.G. and S.B.D. had the initial idea for the experiment. M.C.H. and G.B. fabricated the sample. T.E.M., D.B., H.C.R., D.O., J.A.D., J.W.T., S.R.G. and S.B.D. performed the experiments. T.E.M., D.B. and S.B.D. analysed the data. T.E.M., D.B., J.L., S.R.G. and S.B.D. interpreted the results. T.E.M., D.B., S.R.G. and S.B.D. wrote the paper with contributions from all authors.

Additional information

Supplementary information is available.

Competing interests

The authors declare no competing interests.

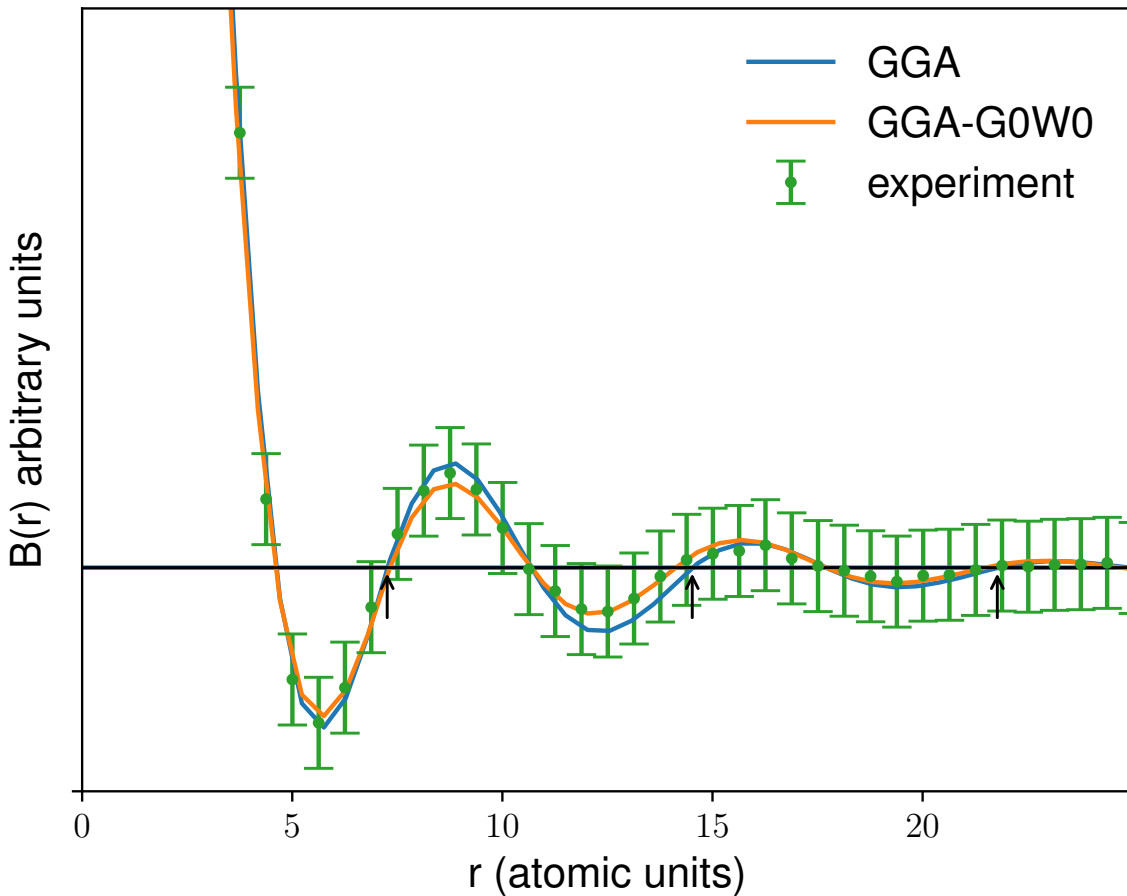


FIG. S1. Reciprocal form factor, $B(r)$, for the weakly correlated (band) insulator, Si, determined from the experimental [110] Compton profile recorded at room temperature, together with those calculated using the generalised gradient approximation (GGA) and GGA- G_0W_0 treatments of exchange and correlation. Error bars indicate statistical errors of one standard deviation. The vertical arrows indicate integer multiples of the [110] lattice constant for which $B(r)$ is zero for an insulator in a one-electron framework.

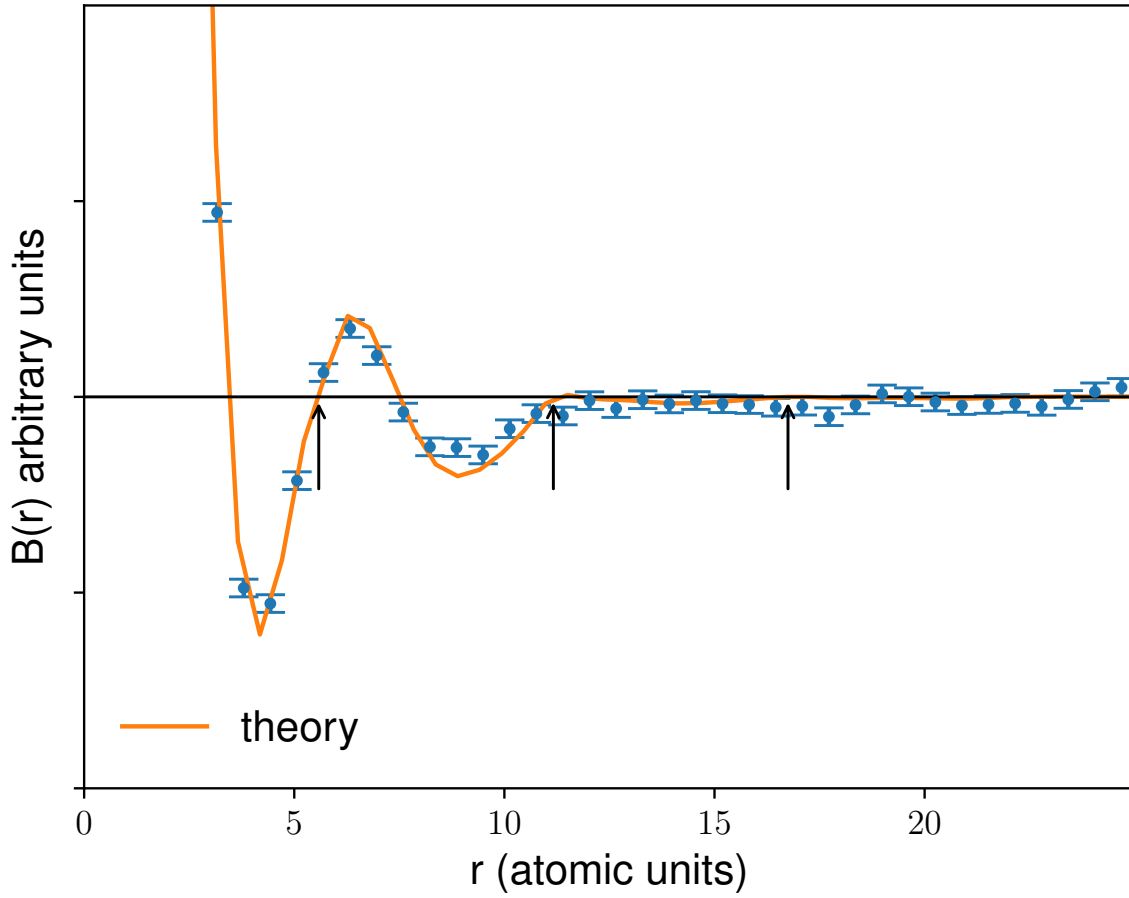


FIG. S2. Reciprocal form factor, $B(r)$, for the strongly correlated (Mott) insulator, NiO, determined from the experimental [110] Compton profile recorded at room temperature, together with that calculated for the antiferromagnetic phase using the meta-GGA SCAN functional for exchange and correlation which produces an insulating (gapped) ground state. Error bars indicate statistical errors of one standard deviation. The vertical arrows indicate integer multiples of the [110] lattice constant for which $B(r)$ is zero for an insulator in a one-electron framework. Clearly, the experiment is very close to zero at these points compared with the situation for SmB_6 (see Fig. 1a of the main text).

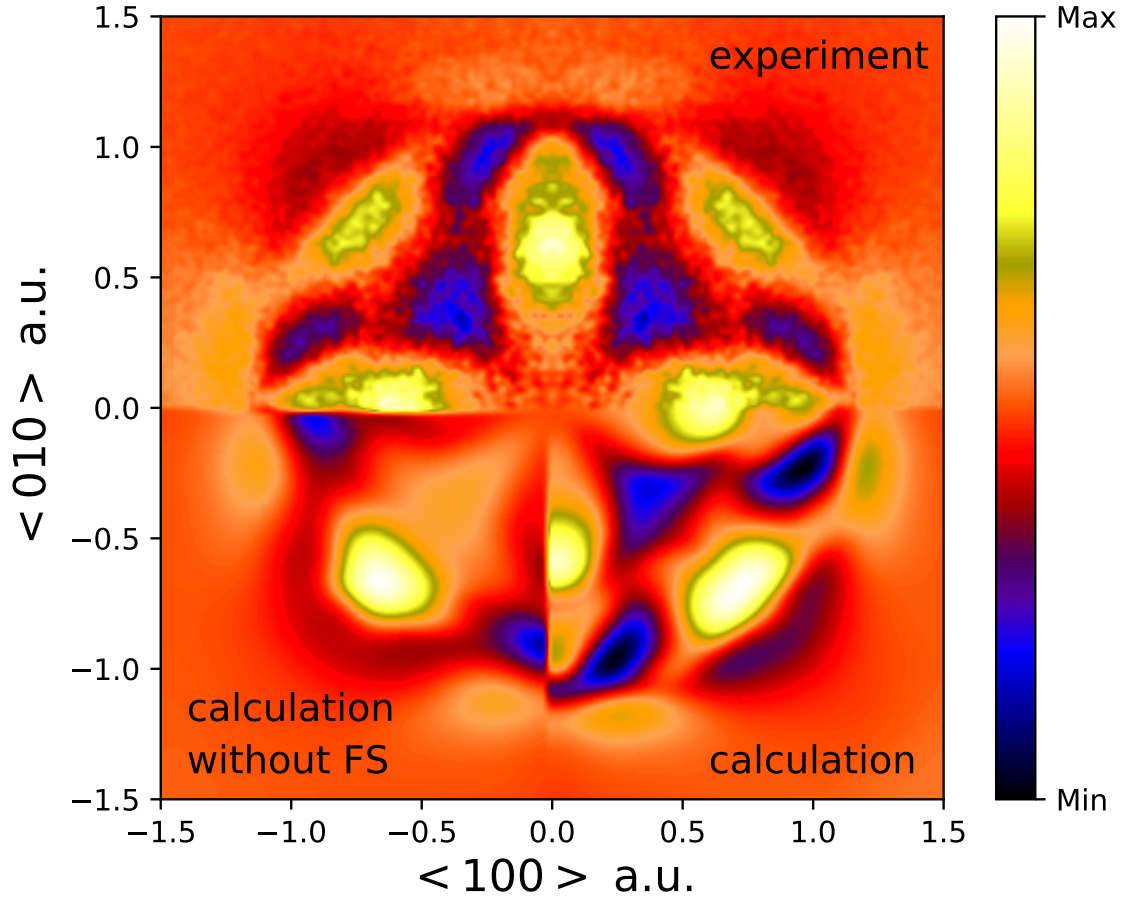


FIG. S3. Radial anisotropy of the experimental (upper half) and calculated (lower right quarter) 2D projected two-photon momentum density, $\rho_{2D}^{2\gamma}(p_x, p_y)$, from 2D angular correlation of (electron-positron) annihilation radiation (2D-ACAR) for LaB₆. The lower left quarter shows the radial anisotropy of $\rho_{2D}^{2\gamma}(p_x, p_y)$ calculated for only the bands which do not cross the Fermi level, E_F , meaning that the Fermi surface contribution has been completely removed from this distribution. Clearly, the ellipsoidal features at the projected set of $\{\frac{\pi}{a}, 0\}$ -points are unambiguously from the Fermi surface. Similar features are observed in the SmB₆ experiment (see main text). The experimental data is from Biasini *et al.* (see Ref. 28 of the main text). The calculated distributions have been convoluted with a 2D Gaussian function approximating the experimental momentum resolution.

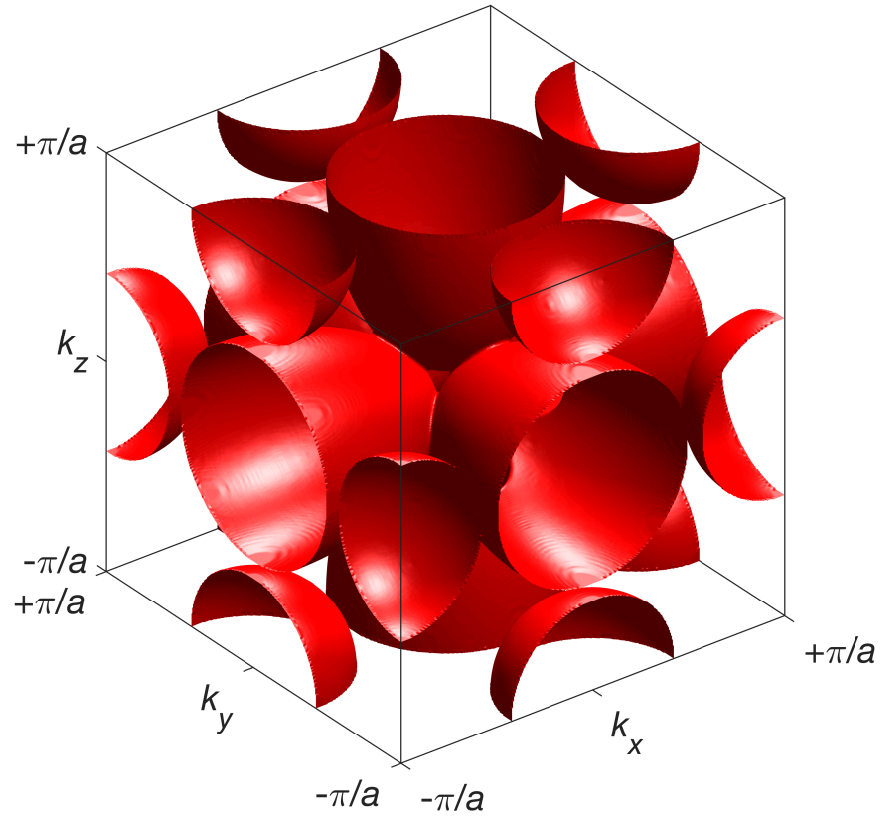


FIG. S4. Best fit Fermi surface model for SmB_6 , consisting of three intersecting ellipsoids centred at the set of $\{\frac{\pi}{a}, 0, 0\}$ -points and three spheres centred at the set of $\{\frac{\pi}{a}, \frac{\pi}{a}, 0\}$ -points. This was determined by varying three free parameters, namely the semi-major and semi-minor axes of the ellipsoid and the radius of the sphere (given in Table 1 of the main text), and minimising the square of the difference between the scaled (see Fig. 2b and Fig. 3 of the main text) experimental $\rho_{2\text{D}}(k_x, k_y)$ for SmB_6 and the same quantity determined from the 3D Fermi surface model convoluted with a 2D Gaussian function approximating the experimental momentum resolution (see Fig. S5 and the upper right quarter of Fig. S6).

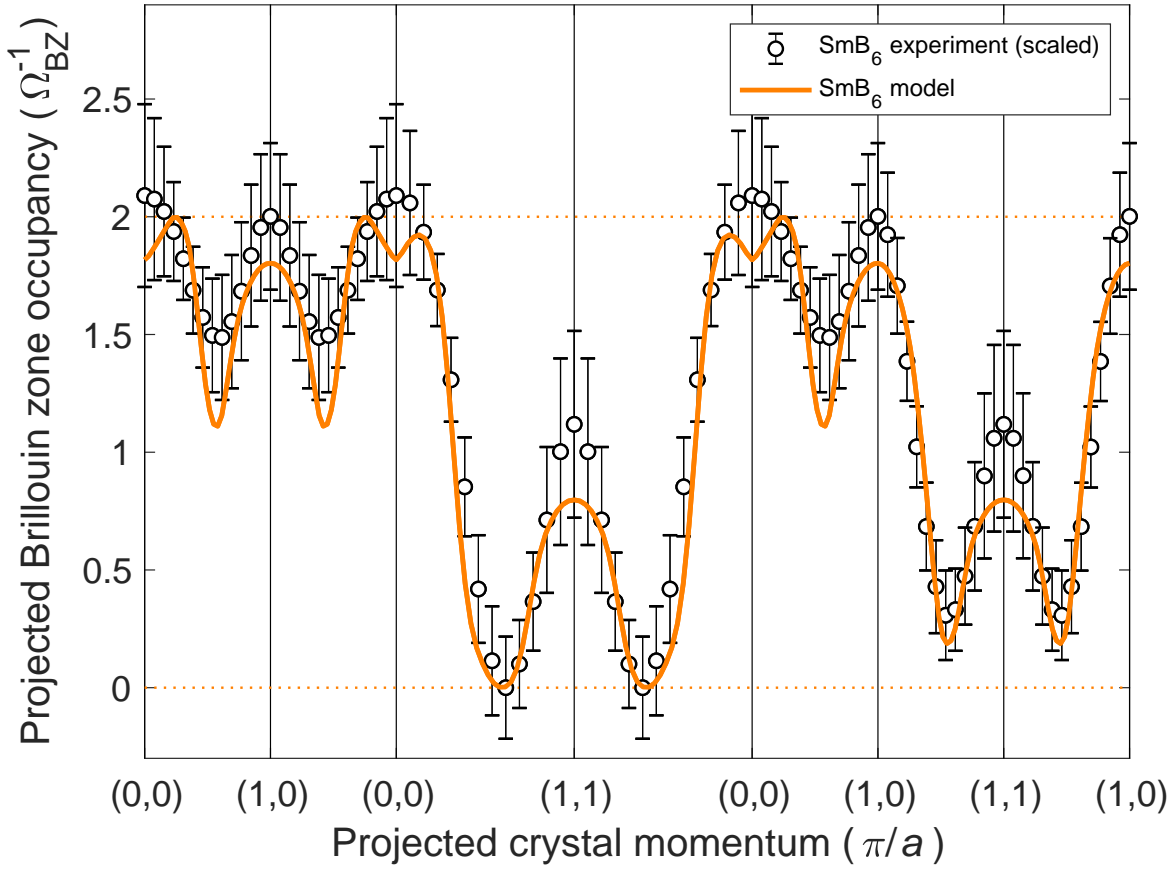


FIG. S5. Sections through the 2D projected occupation density determined from the model Fermi surface (see Fig. S4) compared with sections through the scaled (see Fig. 2b and Fig. 3 of the main text) experimental (001)-plane projected $\rho_{2\text{D}}(k_x, k_y)$ for SmB₆ along selected 2D projected high-symmetry directions. The 2D distribution (shown in the upper right quarter of Fig. S6) determined from the Fermi surface model (see Fig. S4) was convoluted with a 2D Gaussian function approximating the experimental momentum resolution. Error bars indicate statistical errors of one standard deviation. The horizontal dotted lines are $(N_e \pm 1)/\Omega_{\text{BZ}}$ where, for ease of comparison, $N_e = 1$ conduction electron per primitive cell and, here, $\Omega_{\text{BZ}} = (2\pi/a)^2$ is the (001)-plane projected 2D Brillouin zone area.

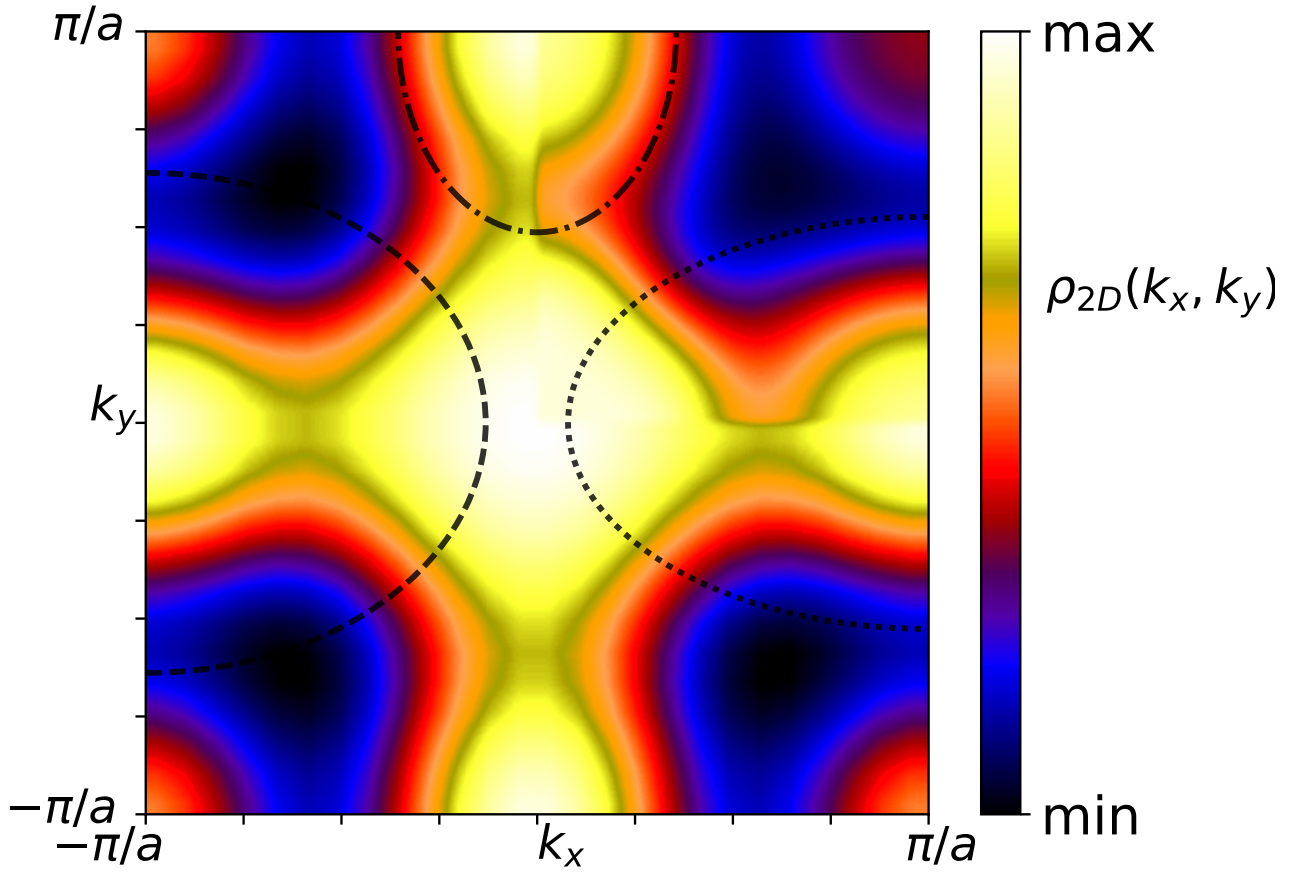


FIG. S6. Experimental 2D projected occupation density, $\rho_{2D}(k_x, k_y)$, for SmB_6 . The upper right quarter shows the comparable distribution determined from the Fermi surface model (see Fig. S4 and S5). Ellipses demonstrating the dimensions of the ellipsoidal component of the remnant Fermi surface are plotted for the Fermi surface model in Fig. S4 and S5 (dotted line, right). Also shown are the small ellipse from ARPES (dot-dashed line, top) and the ellipse for LaB_6 (dashed line, left, from Ref. 29 of the main text). See Table 1 of the main text for the quantitative dimensions.

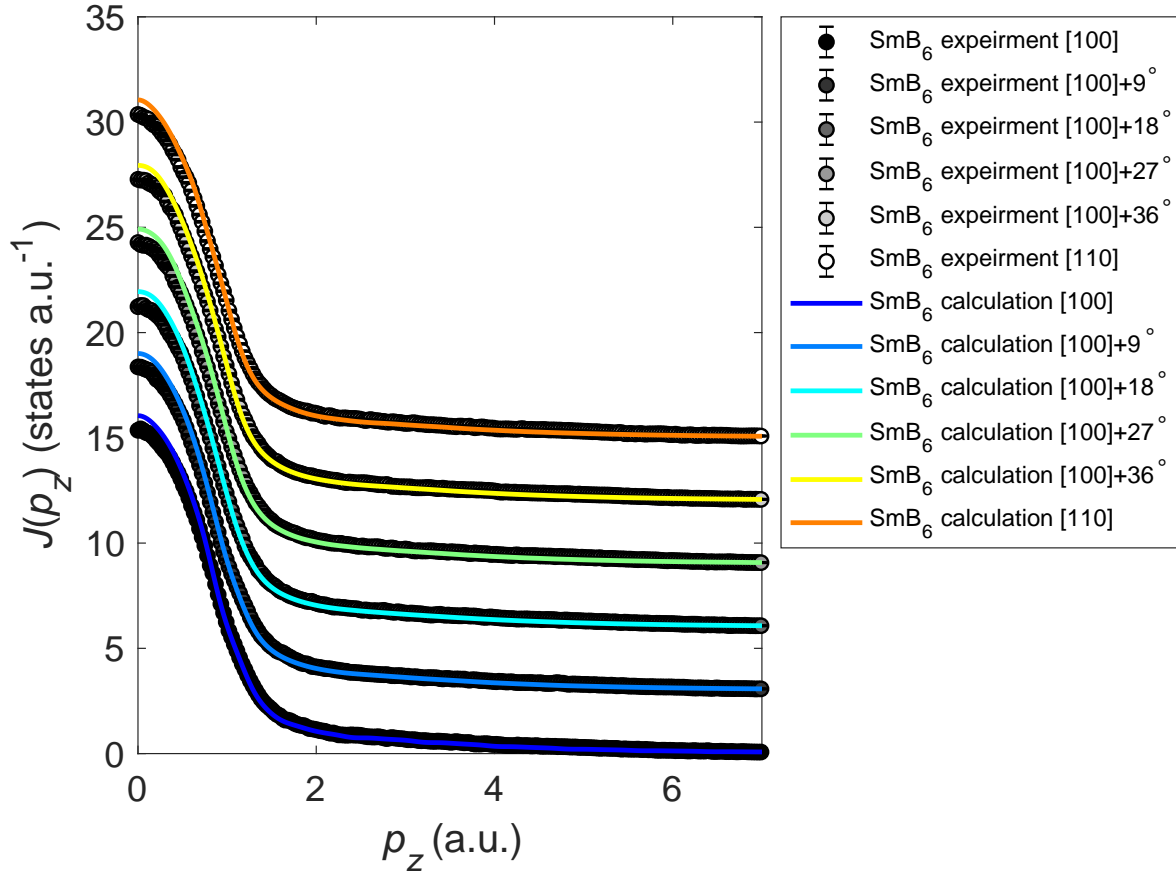


FIG. S7. Experimental and calculated valence electron Compton profiles, $J(p_z)$, for SmB_6 (the isotropic [Xe] core electron configuration has been removed). The calculated profiles have been convoluted with a 1D Gaussian function approximating the experimental momentum resolution. The angles in the legend are from the [100] to [110] directions in the (001)-plane ([110] = [100] + 45°). The profiles have been vertically offset from each other by 3 states a.u.^{-1} for clarity.